

Astrophysical Journal, in press

## A Parsec Scale Accelerating Radio Jet in the Giant Radio Galaxy NGC315

W. D. Cotton<sup>1</sup>

National Radio Astronomy Observatory, 520 Edgemont Rd., Charlottesville VA 22903-2475

L. Feretti and G. Giovannini<sup>2</sup>

Istituto di Radioastronomia del CNR, Via P. Gobetti 101, I-40129 Bologna, Italy.

L. Lara

Instituto de Astrofísica de Andalucía, CSIC, Apdo. 3004, 18080 Granada, Spain.

and

T. Venturi

Istituto di Radioastronomia del CNR, Via P. Gobetti 101, I-40129 Bologna, Italy.

### ABSTRACT

Observations of the core of the giant radio galaxy NGC315 made with VLBI interferometers are discussed in the context of a relativistic jet. The sidedness asymmetry suggests Doppler favoritism from a relativistic jet. The presence of moving features in the jet as well as jet counter-jet brightness ratios hint at an accelerating, relativistic jet. An increasing jet velocity is also supported by a comparison of the jet's observed properties with the predictions of an adiabatic expansion model. On the parsec scale, the jet is unpolarized at a wavelength of 6 cm to a very high degree in clear distinction to the high polarization seen on the kiloparsec scale.

*Subject headings:* galaxies: radio sources

### 1. Introduction

There is growing evidence that the jets observed in the inner regions of powerful extragalactic radio source have highly relativistic flows (see e.g. Urry and Padovani, 1995). The relativistic

---

<sup>1</sup>NRAO is operated by Associated Universities, Inc. under cooperative agreement with the National Science Foundation.

<sup>2</sup>Dipartimento di Fisica, Università di Bologna, via B. Pichat 6/2, I-40127 Bologna, Italy.

effects of such jets will cause their apparent properties to be strongly dependent on the viewing angle. The lines of argument for relativistic motion include side-to-side asymmetries in brightness and polarization, prominence of the core, less X-ray emission than expected from a very high brightness radio core, and apparent superluminal motions in the radio jets. The case for highly relativistic motions in low luminosity sources is less clear. At present, evidence is growing that parsec scale jets are relativistic also in low power sources (see Lara et al., 1997), but a detailed study of more sources is necessary to understand the jet dynamics. In recent years, we have been engaged in a program of studying a complete sample of low power radio sources in order to address this question; this is the ninth paper of this series.

The radio source associated with the galaxy NGC 315 has been well studied since its initial discovery (Davis et al., 1967), and is classified as a low luminosity Fanaroff-Riley type 1 (FR I) radio galaxy. This galaxy is a 12th magnitude dusty elliptical (Ebneter and Balick, 1985) at  $z=0.0167$  with  $H\alpha + [NII]$  emission lines (Marcha et al., 1996). The large scale ( $50'$ ) structure of this radio source (0055+30) has been observed using Arecibo, Westerbork and the VLA (Fanti et al., 1976, Bridle et al., 1976, Willis et al., 1981, Jägers, 1987). On this large scale, the radio source has a long, straight, highly polarized jet (Fomalont et al., 1980, Jägers, 1987) with a sharp bend near the end. The counter-jet is much weaker and has an “S” shaped symmetric bend at its end. The source contains a prominent, peaked spectrum core coincident with the nucleus of the galaxy. This core has been observed using VLBI arrays by Linfield, 1981, Preuss, 1983, and recently by Venturi et al., 1993 at 18, 6 and 3.6 cm. On the basis of high core prominence, low level of nuclear X-ray emission as well as the jet sidedness, Venturi et al., 1993 (but see also Lara et al., 1997) concluded that the jet was highly relativistic, but could not detect the expected motions in the jet in comparison with the images of Linfield, 1981 and Preuss, 1983. The flux density of the core was monitored from 1974 to 1980 by Ekers et al., 1983, but no variations were detected.

At the distance of this source, 1 milliarcsecond (mas) corresponds to 0.47 pc.<sup>3</sup> We present new observations of NGC 315 using the Very Long Baseline Array (VLBA) radio telescope. Many of these data include measurements of the linear polarization.

## 2. Observations and Data Reduction

In this section the details of the observations and the reduction techniques are given. The resultant images are presented in the following section.

The galaxy NGC 315 was observed at wavelengths of 6 and 3.6 cm ( 5 and 8.4 GHz) using the VLBA on 1994 November 14 (total intensity only), and at 6 cm on 1995 October 28 (dual polarization), 1996 May 10 (dual polarization) and 1996 October 7 (dual polarization). These observations are summarized in Table 1. In the November 1994 observations we switched

---

<sup>3</sup> $H_0 = 50 \text{ km sec}^{-1}\text{Mpc}^{-1}$  is assumed throughout the paper.

wavelength every half an hour between 6 and 3.6 cm, obtaining a good uv-coverage at both wavelengths. In the 1995 October observations, the VLA failed to give fringes to the VLBA although internal VLA observations showed no problems. The loss of the VLA seriously reduced the sensitivity which is needed for linear polarization observations and the observations were repeated in 1996 May. During these re-observations, the complete failure of VLBA-St. Croix and serious tape recorder problems at VLBA-Pie Town and VLBA-Mauna Kea reduced the resolution of the data and the observations were rescheduled for 1996 October. This latter session was successful and produced the polarization measurements presented here.

The VLBA data were all correlated on the VLBA correlator in Socorro (NM, USA) and all processing used the NRAO AIPS package. Amplitude calibration was initially done using the standard method employing measured system temperatures and an assumed sensitivity calibration. The VLBA calibration for the VLA was determined from the source to system temperature ratio derived from the VLA data. In the 1995 and 1996 observations, the amplitude calibration was refined using the measured flux densities of the compact calibrator sources (0235+164 in 1995, BL Lac in 1996).

Phase calibration of the 1995 and 1996 data employed the pulsed phase calibration system to remove variations in the difference of the phases of the right- and left-handed polarized signals. All data were globally fringe fitted (Schwab and Cotton 1983) and then self calibrated.

The VLA was used in parallel with the 1995 and 1996 VLBA observations to determine the flux density and polarization of the VLBA calibrators. Because NGC315 is too extended to be used as a phasing calibrator for the VLA, the nearby source 0042+233 was used to periodically phase the VLA antennas. In the 1996 October session, 3C48 was used to calibrate the flux density and polarization angle and 3C84 was used to determine the instrumental polarization for the VLA.

The polarization calibration and imaging followed the general method of Cotton (1993). The polarization calibrator for the 1995 observations was 0235+164 and for the 1996 observations, BL Lac. The 1996 October data was of much higher quality than the previous measurements, so the polarization results presented here are from that session.

Observations of BL Lac were used to derive the cross polarized delay and phase corrections to the VLBA data. The polarization angle corrections were derived independently in each 8 MHz band using the sum of the Q and U CLEAN components from a deconvolution. This procedure makes the plausible assumption that all of the source measured by the VLA was also measured by the VLBA. Instrumental polarization corrections for the VLBA were initially determined from measurements of 3C84 which was assumed to be unpolarized. After it was determined that NGC315 had no detectable polarization with this calibration, corrections to the VLBA instrumental polarization calibration were determined from the NGC315 data assuming the source to be unpolarized in the region to which these data were sensitive.

Table 1: VLBA Observations

Date	Stations	Polarization	BW (MHz)
1994 November 14	PT,KP,LA,FD,NL,BR,OV,HN,MK,SC	single	32
1995 October 28	PT,KP,LA,FD,NL,BR,OV,HN,MK,SC	dual circular	64
1996 May 10	Y,PT,KP,LA,FD,NL,BR,OV,HN,MK	dual circular	64
1996 October 7	Y,PT,KP,LA,FD,NL,BR,OV,HN,MK,SC	dual circular	64

Note. — 1994 November 14 at 6 and 3.6 cm.; other epochs only at 6 cm.;  
Y: Phased VLA; PT: VLBA-Pie Town; KP: VLBA-Kitt Peak; LA: VLBA-Los Alamos; FD: VLBA-Fort Davis; NL: VLBA-North Liberty; BR: VLBA-Brewster; OV: VLBA-Owens Valley; HN: VLBA-Hancock; MK: VLBA-Mauna Kea; SC: VLBA-St. Croix.

### 3. Results

#### 3.1. Monitoring of the arcsecond core flux density

Flux density monitoring of NGC315 at a wavelength of 6 cm by Ekers et al., 1983 from 1974 to 1980 with the WSRT showed no evidence for variations. They found a core flux density of 633 mJy with an rms = 27 mJy. More recent VLA observations show a flare between 1990 and 1995. Flux density measurements at 6 cm are given in Table 2. Many of these measurements are given in this paper for the first time as reported in Table 2. They result from long integrations on the VLA which have been extensively cross calibrated; relative errors are likely lower than the quoted precision. More details on the new VLA data will be given in a future paper, in preparation, on the large scale structure of NGC315. The flux density flare is confirmed also by two observations at 3.6 cm. that give a core flux density of 588 mJy in 1990.92 (Venturi et al., 1993) and of 746 mJy on June 1994 (present paper).

#### 3.2. Total intensity

Calibrated and edited visibility data were used to produce total intensity maps. We used the AIPS package following the standard procedure: a first map was made using the AIPS task IMAGR and several iteration of phase self-calibration followed by a final phase and gain self-calibration were made. In order to exploit the high dynamic range in the 1996 October data, baseline dependent complex gain factors were determined from the NGC315 data by dividing by the Fourier transform of the best self calibrated model and averaging over the entire time of the

Table 2: NGC315 Core Flux Density at 6 cm

Date	Flux Density mJy	Reference
1978.48	620.0	1
1989.28	585.9	2
1995.83	735.2	3
1996.36	694.8	3
1996.77	686.2	3
1996.84	668.1	3
1997.53	688.7	3

Note. — The quoted flux densities for the 1989-1997 measurements have a relative accuracy of better than 0.1 mJy.

References: 1=Bridle et al. 1979, 2=Venturi et al. 1993, 3=this paper.

observations. Since the NGC315 jet is very homogeneous, special care was taken to avoid CLEAN artifacts by using a very low gain factor (0.03) in all the deconvolutions.

### 3.2.1. Total intensity images

In Fig. 1, we present the NGC 315 maps at 6 cm at the four different epochs; details of the images are given in the figure caption. All the images have been rotated by  $-41.5^\circ$  and convolved to the same angular resolution. The radio source morphology, a strong core emission and a straight jet, are in good agreement in all four different images. The noise level in the first three images is similar, although the lack of three telescopes (see Sect. 2) in the May 1996 image produced some residual artifacts and a more irregular zero level in this epoch. Due to the good quality of the data and to the very accurate calibration, the October 1996 image has a noise level a factor 10 lower than the others and a very low level of artifacts.

A comparison of the images in Figure 1 suggests evidence for expansion in the jet. To investigate further the possibility of motions in the jet, enhanced resolution images were obtained from the 6 cm images by restoring the CLEAN components from deconvolution with a Gaussian of the size used for the 3.6 cm image. This was not done for the 1996 May observations due to the lack of long baselines. These high resolution images are presented in Fig. 2 similar to those in Fig. 1. To check if the Clean deconvolution could have created artifacts in the super resolved maps, we

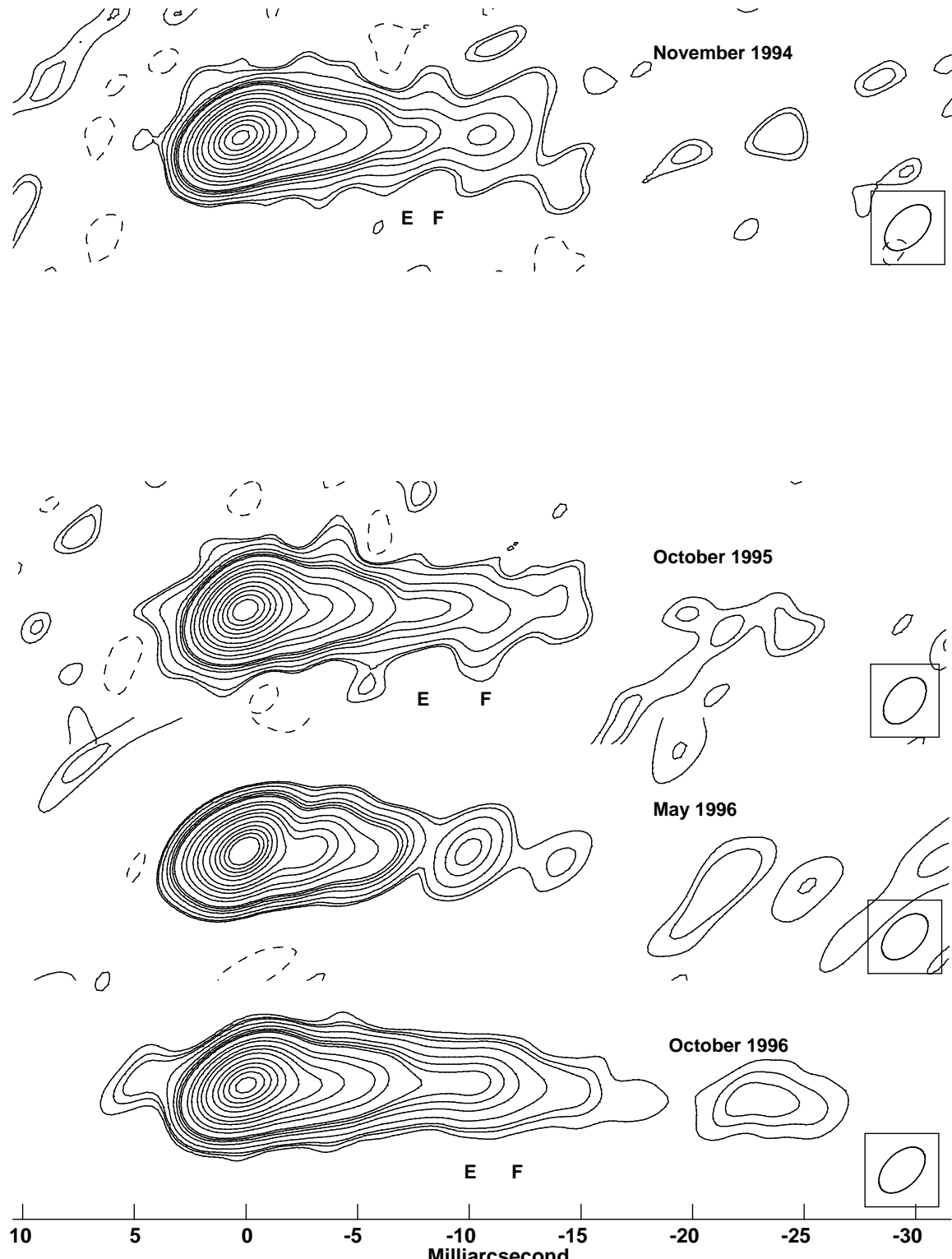


Fig. 1.— The 6 cm images at 4 epochs shown with the same resolution, on the same scale and with similar contour levels. The vertical spacing gives roughly the temporal separation of the images. Labels E and F indicates the location of features. Contour levels are shown at -1, 0.7, 1, 2, 4, 6, 7, 10, 20, 30, 40, 70, 100, 150, 200, 300 and 350 mJy/beam. The 1996 October image has an additional contour at 0.35 mJy/beam. The noise level is 0.4 mJy in the first 2 epochs, 0.5 mJy in the May 1996 map and 0.04 mJy in the last epoch. The images have been rotated on the sky by  $41.5^\circ$ ; the size of the restoring beam ( $2.5 \times 1.5$  mas in position angle  $-48^\circ$ ) is shown in the lower right of each map.

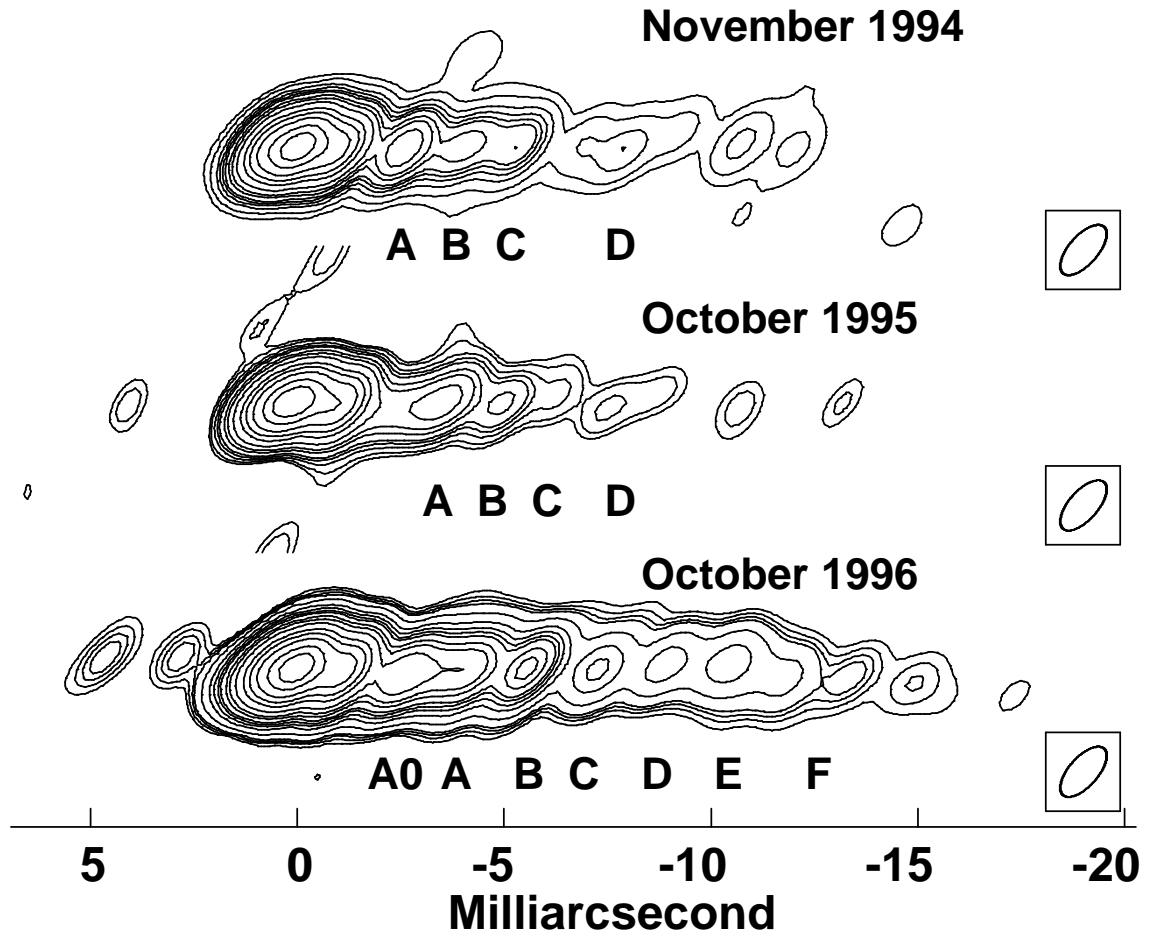


Fig. 2.— The 6 cm images at 3 epochs shown superresolved to the same resolution as the 1994 3.6 cm image and shown on the same scale and with similar contour levels. Labels A0 – F indicates the location of features. Contour levels are shown at 1, 2, 4, 6, 8, 10, 15, 20, 30, 50, 70, 100, 150 and 200 mJy/beam. The lowest contour in the 1995 October image is at 3 mJy/beam and the 1996 November image has additional contours at 0.4, 0.6, and 0.8 mJy/beam. The images have been rotated on the sky by  $-41.5^\circ$ ; the size of the restoring beam ( $1.5 \times 0.7$  mas in position angle  $0^\circ$ ) is shown in the lower right corner.

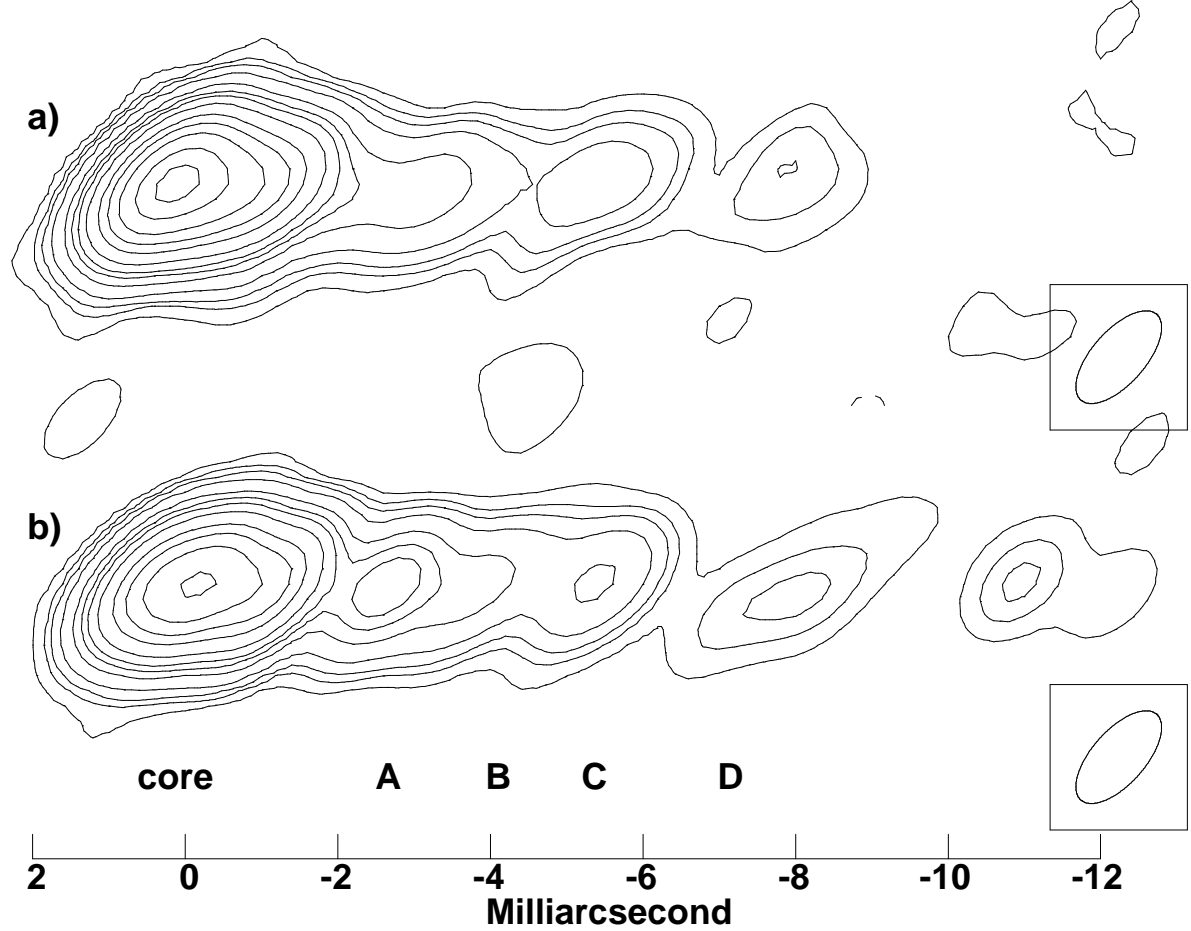


Fig. 3.— a) The 3.6 cm image of NGC 315 from 1994 November. The peak is 345 mJy/beam and contour levels are shown at -1.5, 1.5, 3, 4.5, 7.5, 15, 22.5, 30, 45, 75, 105, 150, 225 and 300 mJy/beam. The image has been rotated on the sky by  $-41.5^\circ$ ; the size of the restoring beam ( $1.5 \times 0.7$  mas in position angle  $0^\circ$ ) is shown in the lower right corner.  
b) The 6 cm image of NGC 315 from 1994 November super-resolved to the resolution shown in a). The peak is 243 mJy and contour levels are the same as in a). The position scale is from the 3.6 cm image. The locations of features discussed in the text are indicated.

compared the November 94 super-resolved map at 6 cm with the same epoch 3.6 cm map (Fig. 3a,b). The strong similarities between the two images of NGC 315 give some confidence in the validity of our procedure.

### 3.2.2. Spectral index image

We used the same epoch observations (November 1994) at 6 and 3.6 cm to produce a spectral index image of the NGC315 jet at the resolution of  $2.5 \times 1.5$  mas. The two images were produced using as similar as possible uv-coverage, with the same gridding and convolved with the same beam. The calibration procedure used on this data does not result in accurate relative registration of the 6 and 3.6 cm images. As the location of the peak of the “core” may be frequency dependent, a weaker but more isolated feature “C” from the images shown in Fig. 3 was used to align the images. With this registration, the peaks of the core at the two wavelengths are not coincident, but slightly shifted (0.3 mas) with the 3.6 cm peak “upstream” of the 6 cm peak. In the following analysis, the center of activity is assumed to be at the location of the 3.6 cm peak.

The trend of the spectral index along the ridge of maximum brightness is shown in Fig. 4. The core region appears strongly self-absorbed and has an inverted spectrum. The spectral index of the jet away from the core is consistent with a relatively constant value of approximately 0.5.

There are several effects that will corrupt the spectral index image. The relatively poorer uv coverage at 3.6 cm wavelength will result in poorer surface brightness sensitivity which will result in incorrectly steep estimates of the spectral index. The rapidly declining surface brightness of the jet will cause any image registration errors to result in systematic variations in the derived spectral index. What can be reliably determined from Fig. 4 is that the core region is optically thick and the jet spectral index steepens to optically thin values.

## 3.3. Polarization

Images of NGC 315 in linearly polarized light do not reveal any polarized emission clearly due to the source, in spite of the low noise level of 0.066 mJy/beam in the Stokes’ Q and U images. Off source apparent artifacts due to imperfect instrumental polarization calibration do not exceed 0.22% of the peak total intensity in the image.

One possible cause of the lack of polarization would be a very high rotation measure in the source in which variations across the bandpass decorrelate the signal. A rotation measure of 82,000 rad/m<sup>2</sup> will cause a 50% decorrelation across our full 32 MHz bandpass. To test for the possibility of very high rotation measure in this source, a polarized intensity image was generated for each of the 64 0.5 MHz channels in the data, and these polarization images were averaged. This scalar averaging of the polarization results in a very slow increase in signal-to-noise ratio

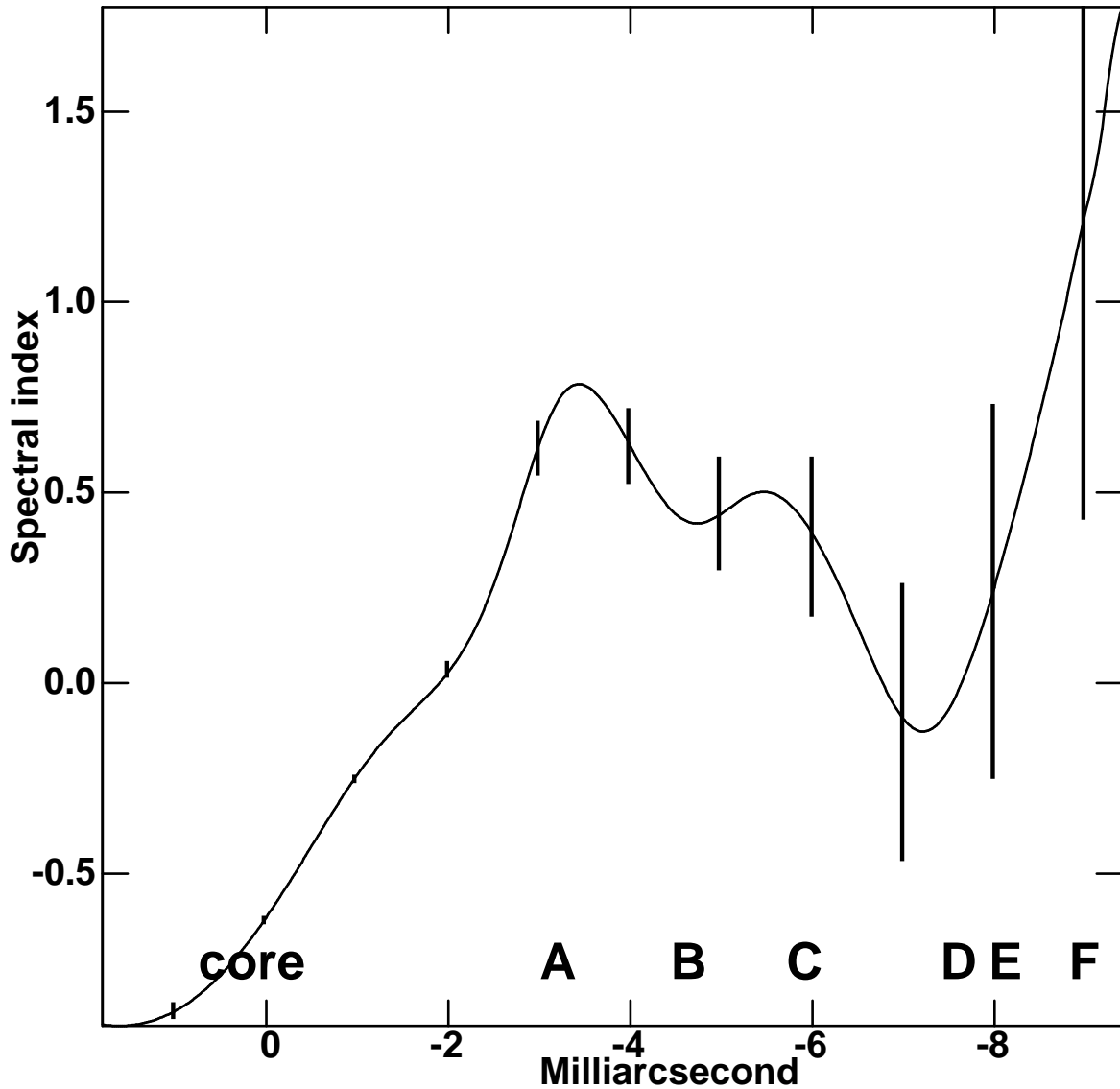


Fig. 4.— The spectral index ( $S = S_0\nu^{-\alpha}$ ) between 6 and 3.6 cm along the ridge line of the jet derived from the 1994 November observations. Resolution used is that of the 6 cm data ( $2.5 \times 1.5$  mas). The locations of features discussed in the text are marked as well as the error bars at selected locations.

Table 3: Upper Limits to Polarization

Distance mas	I mJy	$P_{scalar}$ mJy	$P_{vector}$ mJy	$\%_{scalar}$	$\%_{vector}$
0.0	381.5	0.99	0.18	0.26	0.05
5.5	33.1	1.0	0.10	3.02	0.30
10.25	9.4	1.1	0.29	11.7	3.09

Note. — Distance is from the peak of the core, I is the total intensity,  $P_{scalar}$  is the scalar averaged polarized intensity,  $P_{vector}$  is the vector averaged polarized intensity,  $\%_{scalar}$  is the scalar averaged percent polarization,  $\%_{vector}$  is the vector averaged percent polarization.

with increasing number of channels (the final sensitivity is only a few times that of a single 0.5 MHz channel) but this process is much less sensitive to large rotation measures. The half decorrelation rotation measure is 5,200,000 rad/m<sup>2</sup> for a the scalar averaged polarization image. No polarized emission was detected in the scalar averaged image; this effectively eliminates the possibility of depolarization due to a constant, but very large, Faraday rotation. Table 3 gives upper limits to the source polarization at a number of locations along the jet using both the scalar and vector averaged polarization images. The upper limit quoted is the polarized amplitude at the corresponding image location. High resolution VLA images (to be published elsewhere) indicate 26% polarization at a distance of 700 mas from the core.

## 4. Discussion

### 4.1. Polarization

The low level of linear polarization from the inner region of this radio source could be the result of a very disorganized magnetic field in the jet in its inner few parsecs, Faraday depolarization inside the jet, or Faraday depolarization in a screen in front of the jet. An external Faraday screen must have large fluctuations on size scales smaller than our resolution of about 1 pc (projected). A constant, large Faraday rotation is effectively ruled out by the lack of detected polarization averaged over many 0.5 MHz bands. One possibility for an external depolarizing screen is the Narrow Line Region (NLR). According to Urry and Padovani, 1995 the NLR extends up to  $\sim 32$  pc, corresponding to  $\sim 70$  mas for NGC315. As described above, the jet is probably inclined to the line of sight by approximately  $35^\circ$ , so the line of sight to the inner portion of the jet almost certainly intersects the NLR. Much further from the core, at 700 mas, VLA observations

show that the jet is highly polarized (26%); on this scale the jet is certainly outside of the NLR. Moreover, we have to take in account that the inner 5 - 6 mas are dominated by the core region with an inverted spectrum (see Fig. 4) where the intrinsic polarization is much lower than in the synchrotron transparent regions. High surface brightness sensitivity polarization observations at higher frequencies are needed to determine the extent over which the jet is unpolarized. Unfortunately, polarization VLBI observations of other FRI sources are not yet available for a comparison.

#### 4.2. Nuclear Activity

The radio emission from the core of NGC 315 was relatively constant during the 1970's when it was monitored by Ekers et al., 1983. Since the late 1980's, the core has been more active, with an event apparently peaking in the early 1990's, although during these years the available flux density measurements are too sporadic to properly define the light curve. There is some fluctuation of the brightness of the unresolved "core" component, but most of the additional emission does not appear to be associated with a distinct component. Although the measurements of the core variability are too sparse to allow a correlation with the evolution of the parsec scale structure, they are a clear indication of the activity in this radio galaxy.

#### 4.3. Proper motion

Comparing the images available for NGC 315 (Fig. 1) at different epochs allows the detection of apparent motion. The 1996 May image was not included due to the problems discussed above. The main difficulty in this analysis is that the jet is very homogeneous and the evidence of substructure is not very strong.

The distance from the core of the various features as a function of the epoch is given in Table 4 and shown in Fig. 5. The inner four features in the first two epochs and the inner five in the last epoch are from the super-resolved image (Fig. 2), while point E is from the normal resolution images (Fig. 1). The final feature, F, is the location of a sharp drop in the intensity of the jet. Feature F is not a *knot* in the usual sense but a well defined position in the jet where there is a marked decline in emission, perhaps associated with a new region of activity propagating along the jet. We are aware of the fact that the association of features at the different epochs shown by the lines in Fig. 5 is not the only one possible. However, it is the one which results in the best set of alignments. In this interpretation of Fig. 5, feature A0 is newly emerged from the core.

The measurements shown in Fig. 5 are insufficiently precise to show acceleration or deceleration of a given feature, but the general steepening of the lines down the jet indicates an acceleration of the jet. The average velocity of each feature in the jet is used to derive the  $\beta_{app}$  given in Table 4.

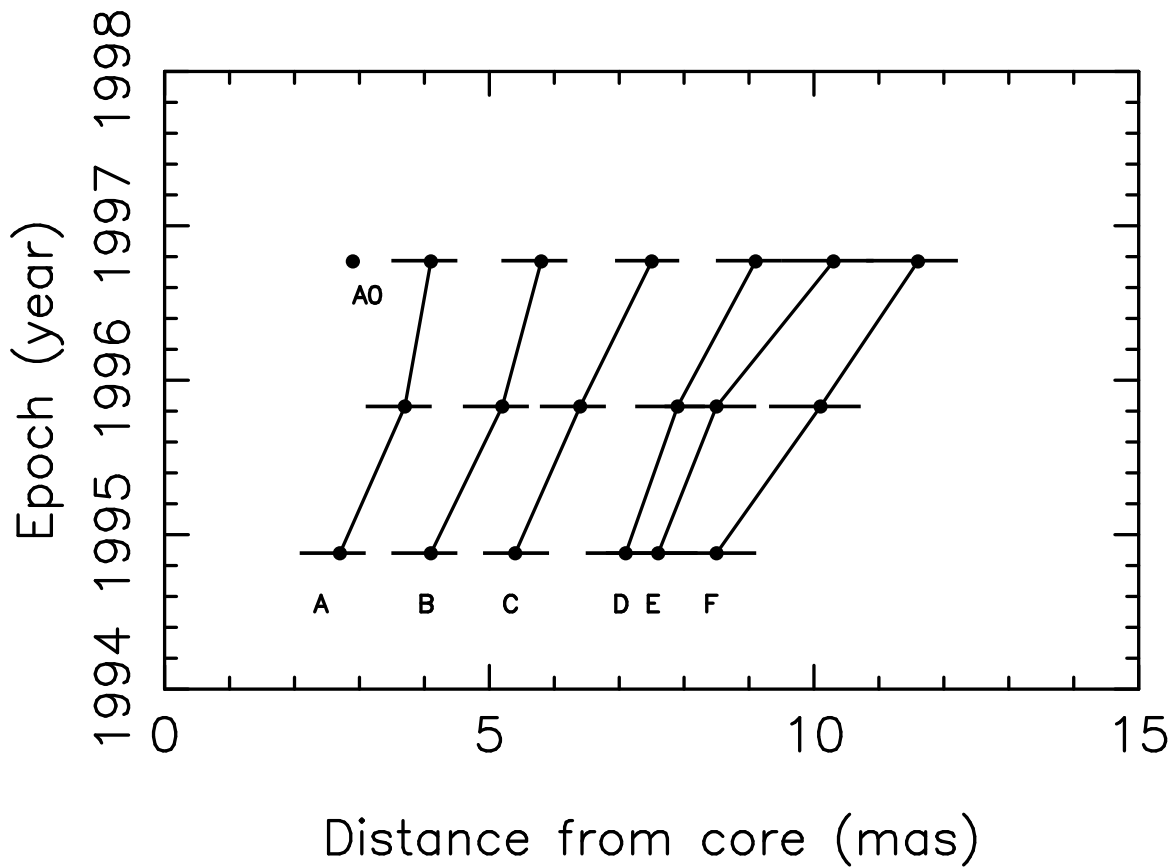


Fig. 5.— The locations of features along the jet in NGC315 at several epochs. The vertical lines indicate the suggested associations. Features A0, A, B, C and D are from the super-resolved images and E and F from the images at normal resolution. The horizontal lines give the approximate uncertainty of the location of the feature.

Table 4: Jet Feature Position and Apparent Velocity

	A0	A	B	C	D	E	F
1994 November	-	2.7	4.1	5.4	7.1	7.6	8.5
1995 October	-	3.7	5.2	6.4	7.9	8.5	10.1
1996 October	2.9	4.1	5.8	7.5	9.1	10.3	11.6
$\beta_{app}$	-	$1.13h_{50}^{-1}$	$1.37h_{50}^{-1}$	$1.70h_{50}^{-1}$	$1.62h_{50}^{-1}$	$2.18h_{50}^{-1}$	$2.51h_{50}^{-1}$

Note. — Distance is from the peak of the 3.6 cm core in mas. A0, A, B, C and D are from super-resolved images; E and F from normal resolution images. The apparent velocity ( $\beta_{app}$ ) in c units is between November 1994 and October 1996;  $h_{50}$  is  $H_0/50$ .

#### 4.4. Jet/Counter Jet ratio

The high quality image of NGC 315 from 1996 October gives indication of a faint counter-jet. The faint and short structure visible in the normal resolution (Fig. 1) and super-resolved (Fig. 2) images is even more evident when natural weighting is used (Fig. 6). A test of the reality of this feature was to perform several iterations of self-calibration disallowing CLEAN components in this region. The apparent counter-jet persisted throughout this procedure and appears to be required by the data. Including this region results in a map with very low noise level as well as a decrease in the level of off-source artifacts. Low resolution images at the other epochs are consistent with a counter-jet, although the noise is too high to confirm its presence.

If the jets are intrinsically symmetric, the jet magnetic field has a random orientation and the asymmetries are entirely due to Doppler beaming, it is possible to determine the component of the jet velocity in our direction using the relation:

$$R = [(1 + \beta \cos \theta) / (1 - \beta \cos \theta)]^{2+\alpha}$$

where  $R$  is the jet/counter-jet brightness ratio,  $\beta$  is the ratio of the jet velocity to the speed of light, and  $\theta$  is the jet angle to the line of sight. (see Giovannini et al., 1994 for a more detailed discussion). We note that NGC 315 shows increasingly symmetric, straight jets on the kpc scale which supports the Doppler favoritism interpretation of the pc scale asymmetries.

A simple interpretation of the jet brightness asymmetries depends on the jet being constant in time, otherwise the time delay between the approaching and receding jets must be included. The “features” in the jet whose motions were derived in a previous section are relatively minor fluctuations on the underlying jet so they may be ignored for this analysis.

As discussed above, the recent flux density outburst in NGC 315 appears to have resulted in a general brightening in the inner jet and a time invariant brightness ratio analysis must ignore the inner 4 mas of the jet. The results of Ekers et al., 1983 suggest that there was an extensive quiescent period prior to the recent outburst.

The image from 1996 October can be used to derive jet/counter-jet ratios along the inner portion of the jet. The inner 4 mas of the jet were avoided due to the very bright core component and the recent outburst discussed above. The spectral index was assumed to have a constant value of 0.5. The measured brightness values are given in Table 5 with the derived values of  $\beta \cos\theta$ . If the angle to the line of sight  $\theta$  is constant, the values shown in Table 5 imply a higher jet velocity, i.e. an acceleration, with increasing distance from the core.

The derived values of  $\beta \cos\theta$  given in Table 5 assumed a constant spectral index whereas Fig. 4 suggests a steepening of the spectrum along the jet. A steepening of the spectral index from 0.5 to 1.5 along the portion of the jet summarized in Table 5 could account for the measured variations in jet/counter jet ratio from a constant velocity jet. As discussed above, the values of  $\alpha$  shown in Figure 4 are subject to substantial error due to imaging difficulties. The optically thick, inner portion of the jet has been excluded from this analysis. A jet spectral index of 1.5 this close to the core would require implausibly rapid energy loss to the radiating electrons; it seems unlikely that the actual spectral steepening could be sufficiently large to produce the increasing brightness ratios observed.

Another possible cause of the jet/counter-jet assymetry could be free-free absorption in an accretion disk around the nucleus as is observed in NGC 1275 (Walker et al., 1998). However, the

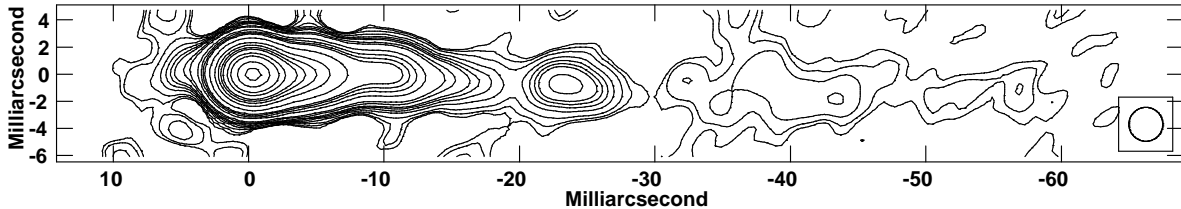


Fig. 6.— The naturally weighted image of NGC315 from the 1996 October data showing the low brightness emission including the counter-jet. The peak brightness is 436 mJy and contour levels are at 0.05, 0.1, 0.2, 0.4, 0.6, 0.8, 1, 1.5, 2, 4, 6, 8, 10, 20, 40, 60, 80, 100, 150, 200, 300 and 400 mJy. The noise level is 0.06 mJy/beam. The image has been rotated on the sky by  $-41.5^\circ$ ; the size of the restoring beam (2.5 mas) is shown in the lower right corner. The position scale is relative to the 3.6 cm peak.

Table 5: Jet Counter-jet brightness ratio

Core distance mas	Jet Brightn. mJy/beam	CJ Brightn. mJy/beam	$\beta \cos\theta$
4.0	75	1.80	0.63
6.0	40	0.65	0.68
7.5	19	0.15	0.76
9.0	13	0.10	0.76
10	13	< 0.06	>0.79

assymmetries from free-free absorption should decrease with distance from the nucleus as the optical depth through the obscuration decreased. Since the observed jet/counter-jet ratio increases away from the core it appears that free-free absorption is not a major contributor to the brightness assymmetries.

#### 4.5. Jet velocity

The discussion above indicates that both the derived motion of features in the jet and the analysis of the jet/counter-jet ratio suggest that the jet is accelerating. From the sidedness ratio (Table 5), we can derive the bulk jet velocity assuming a reasonable orientation of NGC315 with respect to the line of sight. Giovannini et al., 1994, have considered the jet orientation in NGC315 using a number of observational properties such as X-ray emission, core dominance, and the very large linear size of this source as well as the jet/counter-jet brightness ratio and concluded that  $\theta$  is in the range  $30^\circ$  to  $41^\circ$ . We adopt a value for  $\theta$  of  $35^\circ$ . The derived values of the velocity are plotted in Figure 7.

The apparent motion in units of the velocity of light for a relativistically moving feature is given by the relationship:

$$\beta_{app} = \beta \sin\theta (1 - \beta \cos\theta)^{-1}$$

Solving for  $\beta$  gives:

$$\beta = \beta_{app} \times (\beta_{app} \cos\theta + \sin\theta)^{-1}$$

Accurate determination of  $\beta$  depends on knowing the jet's angle to the line of sight as well as the value of  $H_0$ . Using a value of  $35^\circ$  for the jet orientation we note that the bulk and pattern jet velocity are very similar if we assume an Hubble constant  $H_0 = 50 \text{ km sec}^{-1} \text{ Mpc}^{-1}$  (see Fig. 7). This is consistent with the result of Ghisellini et al., 1993, and the general agreement in the literature between the bulk and pattern velocity for superluminal sources (see also Giovannini et al., 1998). In Table 6, we report the derived velocity from the visible proper motion and the

Table 6: Jet Velocity

Core distance pc	$\beta_{j/cj}$	$\beta_{knots}$
3.3	0.77	
3.4		0.75
4.8		0.81
4.9	0.83	
6.2		0.86
6.2	0.92	
7.4	0.92	
7.5		0.85
8.2	>0.96	0.92
9.5		0.95

Note. — Distance is from the peak of the 3.6 cm core in pc de-projected for an angle of  $35^\circ$  and using  $H_0 = 50$ .  $\beta$  is the jet velocity in c units derived using the brightness asymmetry (Col. 2) or the visible proper motion (Col. 3).

brightness ratio assuming  $H_0 = 50 \text{ km sec}^{-1} \text{ Mpc}^{-1}$  and  $\theta = 35^\circ$  at different positions in the jet. The positions are de-projected linear distances in parsec from the core assuming  $\theta = 35^\circ$ .

These two, admittedly weak, derivations of the jet velocity give very nearly the same values of jet velocity and the same acceleration along the jet. Taken together, these two indicators of jet acceleration are stronger evidence than either is individually.

If a value of  $H_0 = 100$  is used, there is substantial disagreement between the two putative indicators of jet velocity, while an intermediate value of  $H_0 = 65$  still gives comparable results. We note that, in any case, an increase in the jet velocity with the distance from the core and a similar acceleration for the bulk and pattern velocity is obtained.

Evidence of the presence of an accelerating jet is given in the literature for a few other sources where jet substructures are found to move at varying velocities and sometimes at varying angles with respect to the line of sight. In the radio galaxy 3C338, Giovannini et al., 1998 found a proper motion with an apparent velocity  $\beta \sim 0.8 \text{ h}_{50}^{-1}$  at 4-5 mas from the core and a slower proper motion at 1.5 mas from the core. Krichbaum et al., 1998, from two 1.3 cm observations of Cygnus A find evidence for an apparent acceleration from  $\beta_{app} \sim 0.2$  to  $\sim 1.2 \text{ h}_{50}^{-1}$  in the region  $1.5 - 3.2 \text{ h}_{50}^{-1} \text{ pc}$  and finally Dhawan et al., 1998 find indication of acceleration along the parsec scale jet in 3C84.

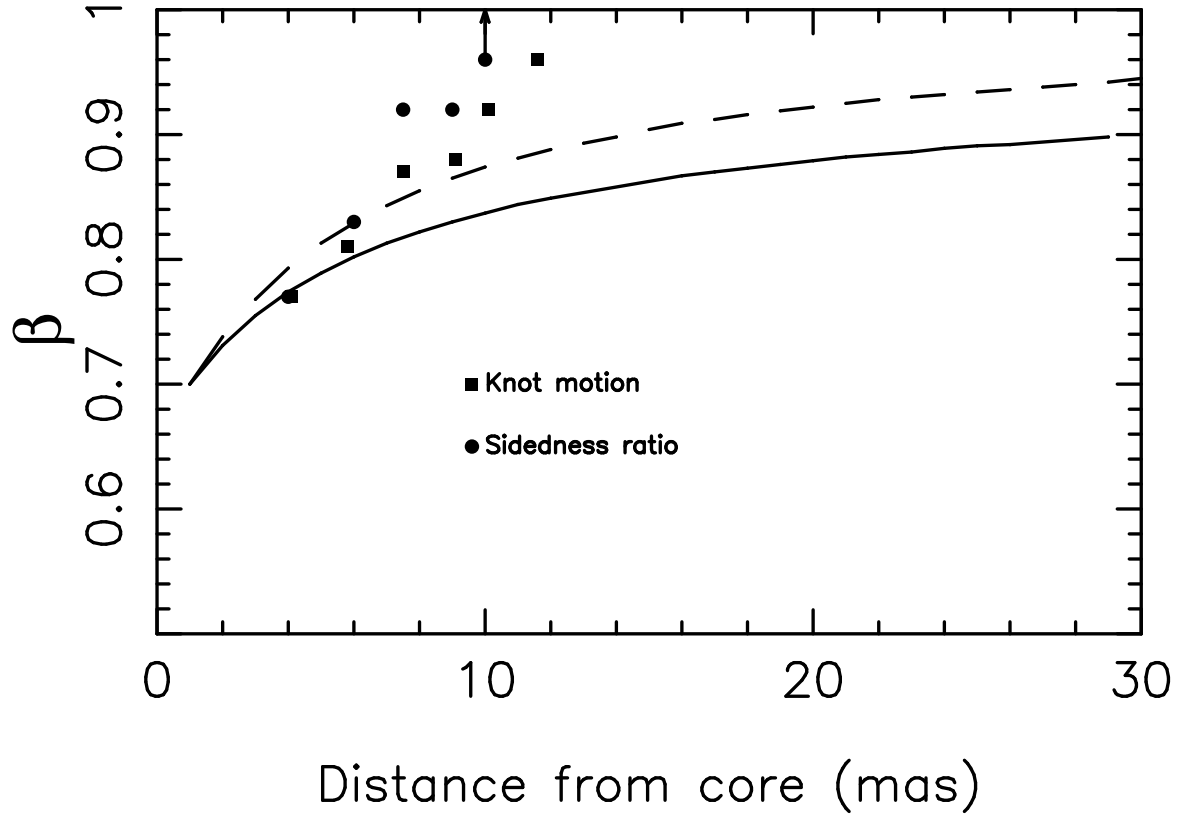


Fig. 7.— The derived jet velocities from apparent knot motions (squares) and jet/counter-jet ratios (circles) at the October 1996 epoch. The orientation to the line of sight is assumed to be  $35^\circ$ ,  $H_0 = 50$  and spectral index  $\alpha = 0.5$ . The lines show the jet velocity  $\beta$  along the jet, obtained from the same epoch, using the adiabatic model. The solid line was obtained assuming a magnetic field oriented parallel to the jet axis, the dashed line uses the assumption of a perpendicular field.

In M87 (3C274), the parsec and kpc scale jet shows a complex velocity field and no unambiguous conclusion can be drawn; however, Junor and Biretta, 1995 find that at very high resolution no proper motion is visible and give a limit of  $0.03c$  for the apparent jet velocity in the inner 0.06 parsec. Biretta et al., 1995 found that velocities measured in the kpc scale jet are much larger than seen at the parsec scale. This evidence for an accelerating pattern speed may be in contrast with the observed jet/counter-jet asymmetry in sources such as M87 (but not in 3C338). Moreover, there are sources with quasi-stationary features near the core but with large jet/counter-jet ratios, suggesting a relativistic bulk flow speed. In NGC315, for the first time, there is evidence of an acceleration of both the pattern and bulk flow velocities.

#### 4.6. An Adiabatic Expansion Model

We have derived potential information about the jet dynamics by applying the simple model in which the jet is adiabatically expanding. Under this assumption, the jet velocity, brightness and radius are related. The functional dependence between these parameters has been discussed in the limit of non-relativistic bulk motion by Fanti et al., 1982, Bicknell, 1984, Perley et al., 1984. The case of relativistic bulk motion is considered by Baum et al., 1997, who obtained the following relationships:

$$\text{Predominantly parallel magnetic field: } I_\nu \propto (\Gamma_j v_j)^{-(2\alpha+3)/3} r_j^{-(10\alpha+9)/3} D^{2+\alpha}$$

$$\text{Predominantly transverse magnetic field: } I_\nu \propto (\Gamma_j v_j)^{-(5\alpha+6)/3} r_j^{-(7\alpha+6)/3} D^{2+\alpha}$$

where  $I_\nu$  is the jet surface brightness,  $\alpha$  is the spectral index,  $r_j$ ,  $v_j$  and  $\Gamma_j$  are the jet radius, velocity and Lorentz factor, and  $D$  is the Doppler factor:  $D = (\Gamma_j(1 - \beta \cos\theta))^{-1}$ .

The jet transverse FWMH (full width at half maximum) and peak brightness at increasing distance from the core were obtained by fitting a Gaussian function to the transverse profiles of images at resolutions of 2.5 mas (see Fig. 6) and 1.8 mas. The parameters were then deconvolved from the CLEAN beam, according to the formula given by Killeen et al., 1986, to get intrinsic quantities. The plot of these parameters is given in Fig. 8. The trend of the FWHM (left panel) shows a smooth increase with distance, with slope  $\sim 0.035$ , corresponding to a constant opening angle of  $\sim 2^\circ$ . The best fit line does not contain the origin of the axes, but gives at the core position (distance = 0) a FWHM of  $\sim 0.2$  mas. In agreement with Venturi et al., 1993, we believe that this is the intrinsic angular size of the radio core. The values of the peak brightness decrease with the FWHM, according to a  $\text{FWHM}^{-5.31}$  law (right panel of Fig. 8). In an adiabatic jet with constant velocity and  $\alpha=0.5$ , the trend implied by the above formulas is  $I_\nu \propto \text{FWHM}^{-4.67}$  and  $I_\nu \propto \text{FWHM}^{-3.17}$ , for the parallel and transverse magnetic field, respectively. The surface brightness observed in the jet decreases faster than can be explained by adiabatic expansion; increasing Doppler dimming of an accelerating, relativistic jet is one possible explanation.

Using the relationships given above, we have modeled the jet brightness and jet FWHM as a

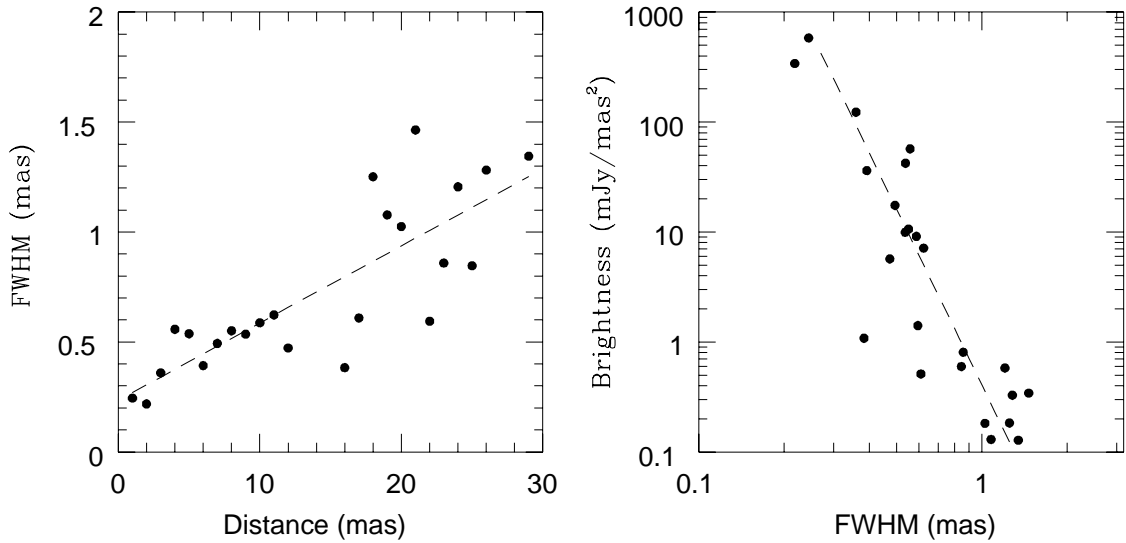


Fig. 8.— Left panel: plot of the deconvolved FWHM of the jet against the distance from the core. The dashed line indicates the best fit to the data, which has been used for fitting the adiabatic model. Right panel: Plot of the deconvolved peak brightness against the deconvolved FWHM of the jet. The dashed line shows the best fit used for the adiabatic model.

function of the distance from the core. To avoid the variations in the measured quantities due to local fluctuations, or to the presence of blobs, we used the parameters obtained from the best fits (see Fig. 8). We assumed a jet spectral index = 0.5, a jet orientation to the line of sight of  $35^\circ$ , and a jet initial velocity (at 1 mas from the core) of  $0.7c$ . We considered the extreme possibilities of a purely parallel and purely perpendicular magnetic field, since this information is not available from the observations. The derived values of  $\beta$  are shown in Fig. 7. The jet velocity increases along the jet up to the distance of 30 mas. The trend of the velocity is not crucially dependent on the orientation of the magnetic field. Also, the use of a lower/higher initial velocity, does not change the overall trend, but only scales it to lower/higher values.

The jet velocity derived from the adiabatic model is in reasonable agreement with the other two estimates shown in Fig. 7 up to a distance of about 10 mas from the core, indicating an acceleration of the jet. After this point, the velocity derived from the adiabatic models are lower than those from the other methods. If this difference is meaningful, then it could indicate a reacceleration of the relativistic particles in the jet in violation of the assumption of an adiabatic jet. The consistency of the adiabatic jet model with the derived proper motion and brightness ratio velocities for the inner portion of the jet further supports the accelerating jet interpretation of the data.

#### 4.7. Where is the Observed Emission from?

There is growing evidence that FRI jets on the kpc scale have highly relativistic spines surrounded by lower velocity sheaths (Laing, 1996). The kpc scale structure of NGC 315 is consistent with such a model and high quality images have been obtained for detailed modeling.

The situation on the pc scale is less clear. A very highly relativistic spine would be invisible to us if the orientation of the jet is indeed  $35^\circ$  from our line of sight and only the slowest moving portions of a spine/sheath jet would be visible. The high degree of depolarization of this source suggests a rich environment for the jet providing material for entrainment and acceleration by a highly relativistic spine.

The data presented here suggest an accelerating jet but doesn't address the question of whether this is merely an acceleration of the outer layers of a mostly invisible, highly relativistic jet or if the jet has not yet accelerated to a highly relativistic state. If we are seeing only the outer layers, the jet should appear to be hollow and, observed with sufficient resolution, is easily distinguished from a strongly center brightened filled jet. Unfortunately, the surface brightness of the fully transversely resolved portions of the jet is below the threshold of the images presented here so this test cannot be performed. Given the difficulties of accelerating a powerful jet many parsecs from the central engine and lacking evidence to the contrary, it seems most probable that the emission in the images in this paper come from the outer layers of a highly relativistic jet.

## 5. Conclusions

We have presented here a detailed study of the nuclear properties of NGC315. We can conclude that:

- a) The nuclear source shows occasional increases in the continuum radio emission indicating very active periods. Unfortunately, the lack of a continuous monitoring does not allow a comparison between the nuclear activity and variation in the parsec scale morphology.
- b) The 6 cm radio structure in the parsec scale jet of NGC315 is quite smooth with some evidence of moving features and a faint counter-jet. When interpreted in terms of a relativistic jet model, apparent motion of the features in the jet, as well as the jet/counter-jet brightness ratio, indicate an acceleration of the jet in its inner 3–10 parsecs. A comparison of the jet’s observed properties with the predictions of a simple adiabatic expansion model further supports the interpretation of an increasing jet velocity. The present data is insufficient to determine if the observed emission is from the entire jet or the slowest portions of an otherwise invisible, highly relativistic jet.
- c) The extremely low upper limits on the polarization of the jet indicate either a very disorganised magnetic field in the inner parsecs of the jet or Faraday depolarization either in the jet or in front of it. A strong candidate for the depolarizing mechanism is Faraday depolarization in the Narrow Line Region, future observations at higher frequency with higher angular resolution will clarify this point.

### Acknowledgements

The authors would like to thank Alan Bridle, Roberto Fanti, Jose-Luis Gomez and Daniele Dallacasa for several helpful discussions. We would also like to thank the staffs of the observatories who participated in these observations and the Socorro correlator staff. L. F. and G. G. acknowledge partial financial support by the Italian Ministry for University and Research (MURST) under grant Cofin98-02-32.

## REFERENCES

Baum, S.A., O'Dea, C.P., Giovannini, G., Biretta, J., Cotton, W.D., de Koff, S., Feretti, L., Golombek, D., Lara, L., Macchetto, F.D., Miley, G.K., Sparks, W.B., Venturi, T., and Komissarov, S. 1997, ApJ, 483, 178

Bicknell, G.V., 1984, ApJ, 286, 68

Biretta, J.A., Zhou, F., and Owen, F.N. 1995, ApJ, 447, 582

Bridle, A. H., Davis, M. M., Meloy, D. A., Fomalont, E. B., Strom, R. G., and Willis, A. G. 1976, Nature, 262, 179

Bridle, A. H., Davis, M. M., Fomalont, E. B., Willis, A. G., and Strom, R. G. 1979, ApJ, 228, L9

Cotton, W. D. 1993, AJ, 106, 1241

Davis, M. M. 1967, *Bull. Astr. Inst. Netherlands*, 19, 201

Dhawan, V., Kellerman, K., and Romney, J.P. 1998, ApJ, submitted

Ebneter, K., and Balick, B. 1985, AJ, 90, 183

Ekers, R. D., Fanti, R., and Miley, G. K. 1983, A&A, 120, 297

Fanti, R., Lari, C., Spencer, R. E., and Warwick, R. S. 1976, MNRAS, 174, 5P

Fanti, R., Lari, C., Parma, P., Bridle, A.H., Ekers, R.D., and Fomalont, E.B. 1982, A&A, 110, 169

Fomalont, E. B., Bridle, A. H., Willis, A. G., and Perley, R. A. 1980, ApJ, 237, 418

Ghisellini, G., Padovani, P., Celotti, A., and Maraschi, L. 1993, ApJ, 407, 65

Giovannini, G., Feretti, L., Venturi, T., Lara, L., Marcaide, J., Rioja, M., Spangler, S. R., and Wehrle, A. E. 1994, ApJ, 435, 116

Giovannini, G., Cotton, W. D., Feretti, L., Lara, L., and Venturi, T. 1998, ApJ, 493, 632

Killeen, N.E.B., Bicknell, G.V., and Ekers, R.D. 1986, ApJ, 302, 306

Krichbaum, T.P., Alef, W., Witzel, A., Zensus, J.A., Booth, R.S., Greve, A., and Rogers, A.E.E. 1998, A&A, 329, 873

Jägers, W. J. 1987, A&AS, 71, 75

Junor, W., and Biretta, J.A. 1995, AJ, 109, 500

Laing, R. A. 1996, in Energy Transport in Radio Galaxies and Quasars, eds. P. E. Hardee, A. H. Bridle and J. A. Zensus, ASP Conference Series, 100. 241

Lara, L., Cotton, W.D., Feretti, L., Giovannini, G., Venturi, T., and Marcaide, M. 1997, *ApJ*, 474, 179

Linfield, R. 1981, *ApJ*, 244, 436

Marcha, M. J. M., Browne, I.W.A., Impey, C.D., and Smith, P.S. 1996, *MNRAS*, 281, 425

Perley, R.A., Bridle, A.H., Willis, A.G., 1984, *ApJS*, 54, 291

Preuss, E. 1983, in *Astrophysical Jets*, ed. A. Ferrari & A. G. Pacholczyk (Dordrecht: Reidel), 1

Schwab, F. R. and Cotton, W. D. 1983, *AJ*, 88, 688

Urry, C.M., and Padovani, P. 1995, *PASP*, 107, 803

Venturi, T., Giovannini, G., Feretti, L., Comoretto, G., and Wehrle, A. E. 1993, *ApJ*, 408, 81

Willis, A. G., Strom, R. G., Bridle, A. H., and Fomalont, E. B. 1981, *A&A*, 95, 250

Walker, R. C., Kellermann, K. I., Dhawan, V., Romney, J. D., Benson, J. M., Vermeulen, R. C., and Alef, W. 1998, in *IAU Colloquium 164: Radio Emission from Galactic and Extragalactic Compact Sources*, ASP Conference Series, 114, J. A. Zensus, G. B. Taylor, J. M. Wrobel (eds.), 133